Soil and Atmospheric Controls on the Land Surface Energy Balance: A Generalized Framework for Distinguishing Moisture#Limited and Energy#Limited Evaporation Regimes

Soil and atmospheric controls on the land surface energy balance: A generalized framework for distinguishing moisture- and energy-limited evaporation regimes

Erfan Haghighi[1†], Daniel J. Short Gianotti[1], Ruzbeh Akbar[1], Guido D. Salvucci[2], and Dara Entekhabi[1]

[1]Department of Civil and Environmental Engineering, Massachusetts Institute of Technology, Cambridge, MA, USA

[2]Department of Earth and Environment, University of Boston, Boston, MA, USA

[†]Corresponding Author:

Erfan Haghighi
Dept. of Civil and Environmental Engineering
Massachusetts Institute of Technology
Building 48-102
77 Massachusetts Ave.
Cambridge, MA 02139
United States

E-mail address: erfanh@mit.edu

This is the author manuscript accepted for publication and has undergone full peer review but has not been through the copyediting, typesetting, pagination and proofreading process, which may lead to differences between this version and the Version of record. Please cite this article as doi:10.1002/2017WR021729.

Key Points (140 characters):

- Evaporative fraction-soil moisture (EF-SM) relationship is a multi-dimensional function with dependence on other environmental factors
- We propose a generalized EF framework that accounts for surface and micrometeorological conditions influencing the EF-SM relationship
- The framework offers analytical estimates of a critical SM marking transitions between moisture- and energy-limited evaporation regimes

Abstract (250 words)

The relationship between evaporative fraction (EF) and soil moisture (SM) has traditionally been used in atmospheric and land-surface modeling communities to determine the coupling strength between land surfaces and the atmosphere in the context of the dominant evaporation regime (energy- or moisture-limited). However, observation-based analyses suggest that EF-SM relationship in a given region can shift subject to other environmental factors, potentially influencing the determination of the dominant evaporation regime. This implies more complex dependencies embedded in the conventional EF-SM relationship and that in fact it is a multi-dimensional function. In this study we develop a generalized EF framework that explicitly accounts for dependencies on other environmental conditions. We show that large scatter in observed EF-SM relationships is primarily due to the projection of variations in other dimensions, and propose a normalization of the EF-SM relationship accounting for the dimensions and dependencies not included in the conventional relationship. In this first study we focus on bare soil conditions in order to establish the basic theoretical framework. The new generalized EF framework provides new insights into the origin of transition between energy- and moisture-limited evaporation regimes (marked by a critical SM), linked to soil type and meteorological input data (primarily wind speed and air temperature, but not solar radiation) dominating the evolution of land surface temperature and thus the relative efficiency of surface energy balance components during surface drying. Our results offer new opportunities to advance predictive capabilities quantifying land-atmosphere coupling for a wide range of present and projected meteorological input data.

Keywords: Evaporative fraction (EF); Soil moisture (SM), EF-SM relationship; Evaporation regime; Land-atmosphere coupling.

1. Introduction

Land surface energy balance is a key factor for the climate system, regulating hydrometeorological processes taking place near the Earth's critical zone where the subsurface is closely coupled with the atmosphere (Brooks et al., 2015). Of particular interest is the role of land surface water availability (hereafter referred to as soil moisture) in partitioning incoming radiative energy into sensible and latent heat fluxes at the land surface, which, in turn, affects temperature and humidity in the lower atmosphere (Entekhabi et al., 1996; Gu et al., 2006; Koster et al., 2009; Schwingshackl et al., 2017; Seneviratne et al., 2006, 2010, 2013; Whan et al., 2015). Soil moisture (SM) evolution itself is forced by available energy and precipitation resulting in (positive or negative) feedbacks with the atmosphere (Guillod et al., 2015; Tuttle & Salvucci, 2016). Such dynamic feedbacks between the land surface and the atmosphere can contribute to extended precipitation and temperature anomalies, and can amplify climate extremes such as heat waves and drought (Fischer et al., 2007; Gu et al., 2006; Hauser et al., 2016; Hirschi et al., 2011; Miralles et al., 2014; Mueller & Seneviratne, 2012). Given the critical role of land-atmosphere water and energy exchange in modulating hydrologic and climatic conditions, it is imperative to quantitatively represent energy partitioning at the land surface and characterize its dependence on SM.

Land surface energy balance components include radiative exchanges with the atmosphere, ground heat flux and turbulent exchanges of latent and sensible heat fluxes to the lower atmosphere. The abundance or lack of water at the surface determines the partitioning of available energy among latent and sensible heat fluxes. The partitioning is a critical factor in the efficacy of dissipating heat away from the surface (Bateni & Entekhabi, 2012; Gentine, Polcher, et al., 2011), and is represented as the latent heat flux normalized by the sum of latent and sensible heat fluxes, referred to as evaporative fraction (EF). It is also equivalent to latent heat flux fraction of the available energy in land surface energy balance. The EF

diagnostic is a useful measure for energy partitioning at the land surface which has extensively been used in atmospheric and land-surface modelling communities to determine the strength of land-atmosphere coupling in the context of the dominant evaporation regime (energy- or moisture-limited) (Dirmeyer et al., 2000; Koster et al., 2009; Santanello et al., 2011; Seneviratne et al., 2010).

Inspired from the seminal studies of Budyko (1974) and Eagleson (1978), the relationship between EF and SM reveals two distinct hydroclimatic regimes characterizing land-atmosphere water and energy interchange: (1) a wet regime in which SM content is high such that land evaporation (and the resulting latent heat flux) is governed by the incoming radiation and is thus referred to as energy-limited, and (2) a transitional regime with lower SM content in which land evaporation increases/decreases in response to increasing/decreasing SM content (i.e., moisture-limited). Overall, the two distinct evaporation regimes determine how strongly SM constrains land evaporation and resulting feedbacks to the atmosphere (i.e., weak or strong land-atmosphere coupling). We note that SM in this study refers specifically to land surface water availability within a shallow surface layer (as opposed to the root-zone SM); nevertheless the EF-SM relationship is also evident in the conditions of the surface SM layer which is correlated with the profile SM (at least for mean climatological conditions and except for very dry conditions) (Crow et al., 2017; Hirschi et al., 2014; Qiu et al., 2016; Schwingshackl et al., 2017).

Implicit in the EF-SM metric is the assumption that the available SM is readily evaporated given sufficient available energy at the land surface, and is neither restricted nor aided by near-surface boundary layer interactions (including subsurface hydraulic properties and above-surface diffusive mechanisms constraining vapor exchanges across the land-atmosphere interface). However, observational studies suggest that the EF-SM relationship is

not unique such that the dominant evaporation regime in a given region may vary substantially with land surface and atmospheric variability (Bagley et al., 2017; Bertoldi et al., 2007; Williams & Torn, 2015; Zscheischler et al., 2015) and/or following precipitation or radiation anomalies (Ford et al., 2014; Koster et al., 2004, 2006, 2009; Schwingshackl et al., 2017). These imply that the conventional EF-SM relationship (exclusive of surface and meteorological conditions) is embedded in more complex dependencies (Gentine et al., 2007; Gentine, Entekhabi, et al., 2011; Gu et al., 2006) and that in fact it is a multi-dimensional function. An illustrative example is shown in Figure 1 demonstrating variations in half-hourly EF data (based on flux tower measurements of latent and sensible heat fluxes) with meteorological variables.

Figure 1 shows the EF-SM relationship observed at a semi-arid site during five Spring and Summer seasons. Also included are the histograms of key micrometeorological factors, including incoming solar radiation, screen-height air temperature, air relative humidity and wind speed. The blue-colored data are inclusive of all environmental conditions, resulting in wide scatter in the EF-SM relationship. The red and yellow-colored data are for particular combinations of solar radiation, relative humidity, air temperature and wind speed. The EF-SM relationships for these two subsets of data show the expected form of rising EF with SM that asymptotes for well-watered conditions. The two subsets (conditioned on environmental conditions) however have distinct forms. The conclusion is that the original (all-inclusive) blue-colored EF-SM scatter is composed of projections of many different dependencies not accounted for in a two-dimensional plane. Thus, the EF-SM relationship is not unique even for the same location and in fact it is a multi-dimensional function, with other dimensions including micrometeorological factors (i.e., solar radiation intensity, air temperature, relative humidity and wind speed) and potentially many others (Gu et al., 2006). In this particular example, the incoming solar radiation factor in the two subsets is the most distinct. Even

though EF is normalized by available energy, the solar radiation factor effect is prominently evident (Ford et al., 2014). The inset conceptual graphic depicted in the EF-SM plot of Figure 1 shows how the solar radiation dimension (for example) will contain different EF-SM relations. If all data are collapsed onto the two-dimensional EF-SM plane without consideration of other dependencies, large scatter and incoherent relationships emerge.

The main goal of this study is to analyze the underlying causes of large scatter in EF-SM observations and demonstrate that the relationship is actually part of a multi-dimensional system with further dependencies on other environmental factors. We show that these factors can be taken into account explicitly through surface energy balance. Equations capturing the multi-dimensional system are developed and we normalize the EF-SM relationship such that the projection of the other dimensions onto the EF-SM plane does not result in scatter. Instead a universal functional form is derived which distinguishes between the moisture-limited and energy-limited evaporation regimes. Thus, the objectives of this study are twofold: (1) to establish a physically based framework for energy partitioning at the land surface explicitly incorporating coupled SM-atmospheric controls, and (2) to extend the results to develop a new generalized EF-based metric (with improved predictive capabilities) quantifying changes in the coupling strength between the land surface and the atmosphere *a priori*.

We introduce here a generalized EF framework (Figure 2) characterizing the coupling strength between land surfaces (specifically bare soils, in this study) and the atmosphere, with explicit account of the important role of varying surface and meteorological conditions in regulating land surface energy partitioning (Aminzadeh & Or, 2014; Bateni & Entekhabi, 2012; Shahraeeni & Or, 2010) and thus EF-SM relationships. In particular, we implement a linearized form of the surface energy balance equation that incorporates an analytical pore-

scale soil evaporation model (Haghighi, 2015; Haghighi & Or, 2013) linking SM content and atmospheric properties jointly affecting heat and mass exchange rates at the surface. This enables us to predict *a priori* the evolution of land surface temperature during surface drying, thereby quantifying the surface energy partitioning between sensible and latent heat fluxes. Capitalizing on the advantages of this analytical setting, we derive a novel theoretical expression for EF in the form of relative efficiencies of surface energy balance components as well as climatological driving forces, providing new insights into the two key variables characterizing multi-dimensional EF-SM relationships: (1) a potential EF (EF_{pot}) indicating the equilibrium value EF takes under non-limiting SM (θ) for a given set of meteorological boundary conditions, and (2) a critical SM (θ^*) that marks the onset of transition between energy- and moisture-limited evaporation regimes (see Figure 2).

We discuss potential benefits of these newly derived metrics for improving predictive capabilities of the conventional evaporation regime conceptualization, with results evaluated for field experiment data sets. In this study we forward the theoretical framework with the bare soil case. The vegetated surface case has more parameters and it is more complicated. In this first introduction of the conceptual framework, we work with the simpler (but more critical) bare soil case, where ignoring near-surface atmospheric variability can lead to significant errors (>50%) in EF estimates (Bertoldi et al., 2007), and use observations from field sites with very sparse vegetation.

2. Theoretical Development

2.1. Analytical Description of EF Dependence on Land Surface Temperature

The land surface temperature is the state variable of surface energy balance and hence contains information on the partitioning of available energy at the surface among various surface energy balance components (i.e., sensible, latent and ground heat fluxes as well as

outgoing longwave radiation), reflecting their relative contribution (Aminzadeh & Or, 2014; Bateni & Entekhabi, 2012). We derive an estimate of equilibrium land surface temperature that forms the basis for a mechanistic description of energy partitioning at the land surface. The surface energy balance during equilibrium evaporation from the land surface is expressed as (Monteith, 1981; Penman, 1948):

$$Rn - G = \lambda E + H \tag{1}$$

where $\lambda = 2.45 \times 10^6$ (J kg^{-1}) is the latent heat of vaporization. A list of symbols used in this study is given in Table 1. Equation (1) serves as a boundary condition for energy exchange processes at the land surface, determining how available energy (i.e., net radiation flux minus ground heat flux, $Rn - G$) is partitioned between latent (λE) and sensible (H) heat fluxes when an equilibrium temperature achieved by the land surface (i.e., no storage in the surface layer) (Monteith, 1981).

The net radiation flux Rn (W m^{-2}) is the primary source of energy intercepted at the land surface, and is the sum of incoming and outgoing shortwave and longwave radiation fluxes according to:

$$Rn = (1 - \Lambda) \cdot R_s + \sigma \varepsilon_s \varepsilon_a T_a^4 - \sigma \varepsilon_s T_s^4 \tag{2}$$

where Λ (-) is the surface albedo, R_s (W m^{-2}) is the incoming solar radiation, and $\sigma \varepsilon_a T_a^4$ and $\sigma \varepsilon_s T_s^4$ are incoming and outgoing longwave radiation fluxes, respectively, with $\sigma = 5.67 \times 10^{-8}$ (W m^{-2} K^{-4}) the Stefan-Boltzmann constant, ε_a and ε_s (-) the air and surface thermal emissivity, respectively, and T_a and T_s (K) air temperature at a reference height and equilibrium surface temperature, respectively. We note that the effective atmospheric emissivity ε_a could be obtained as a function of near-surface air temperature and vapor

pressure under clear sky condition (Brutsaert, 1975), and corrected for cloudiness using the method proposed by Crawford & Duchon (1999).

Using the resistance analogy based on Ohm's law, ground heat flux G (W m^{-2}) and sensible heat flux H (W m^{-2}) can be expressed in terms of the near surface gradient of temperature from the land surface (T_s) to the deep ground ($\bar{T}$, approximated by monthly-averaged air temperature) and to the atmosphere (T_a), respectively, as:

$$G = \frac{\rho c_p}{r_g} \cdot \left(T_s - \bar{T} \right) \tag{3}$$

$$H = \frac{\rho c_p}{r_{aH}} \cdot \left(T_s - T_a \right) \tag{4}$$

where ρ (kg m^{-3}) is the air density, c_p (J kg^{-1} K^{-1}) is the air specific heat at constant pressure, and $r_g = \rho c_p Z_T / K_s$ and $r_{aH} = \rho c_p \delta / K_a$ (s m^{-1}) are the ground heat flux resistance and the aerodynamic resistance to sensible heat flux from the surface to the overlaying air layer, respectively. Z_T (m) is an effective thermal depth that senses surface temperature fluctuations and ranges from 10 to 30 mm for practical conditions (Gao et al., 2017; Li et al., 2016; Shahraeeni & Or, 2011), and $\delta \approx 21\nu / u_*$ (m) is the thickness of an aerodynamic layer close to the surface (termed viscous sublayer) that underlies turbulent air boundary layer and sets the boundary conditions for heat and water vapor transfer by thermal conduction and molecular diffusion, respectively (Haghighi et al., 2013; Haghighi & Or, 2013, 2015b). ν (m^2 s^{-1}) is the air kinematic viscosity and u_* (m s^{-1}) is the friction velocity approximated by $0.1 \times U_a$ for bare soils (Haghighi & Or, 2013, 2015a), with U_a (m s^{-1}) the wind speed at the reference height. K_s and K_a (W m^{-1} K^{-1}) are the soil and air thermal conductivity, respectively.

Implicit in (3) is the assumption of a linearized soil temperature profile, originally varying exponentially with soil depth (Bateni & Entekhabi, 2012; Shahraeeni & Or, 2011), across the relatively shallow surface soil layer of thickness Z_T where more dramatic temperature changes (from T_s to $\bar{T}$) occur. We also note that (4) assumes a fully mixed turbulent regime above the viscous sublayer such that air temperature at the border of the viscous sublayer is similar to that at the reference height. According to the surface renewal theory (Danckwerts, 1951; Higbie, 1935), intermittent sweep and ejection of turbulent eddies above the viscous sublayer (termed renewal events) would result in scalar transfer coefficients much higher than the corresponding ones across the viscous sublayer. This, in turn, enables the assumption that vertical gradients in scale quantities (from their values at the surface to those in the ambient air at the reference height) are steepest across the viscous sublayer, and that heat and mass transfer across the viscous sublayer is the rate-limiting process controlling surface fluxes (Haghighi & Or, 2013, 2015b; Katul et al., 1996; Paw U et al., 1995). We note that the assumption of a well-mixed turbulent atmosphere (i.e., $T_\delta = T_a$) irrespective of atmospheric stability conditions could result in significant errors (Haghighi & Or, 2015b), and is basically applicable to unstable atmospheric conditions. This is the case for most practical conditions of interest here with $H > 0$ (i.e., $EF < 1$) that facilitates rapid vertical movement of turbulent eddies (i.e., unstable atmospheric boundary layer). The numerical procedure proposed by Haghighi and Or (2015b) can be used to correct this top boundary condition as a function of atmospheric stability parameter.

Latent heat flux λE (W m^{-2}) is the key component of the surface energy balance equation providing direct links to the coupled SM-atmospheric controls on land surface energy partitioning and the resulting surface temperature field as the land surface gradually dries. Here, we use a pore-scale description of diffusive water vapor fluxes from discrete pores

(Haghighi et al., 2013; Shahraeeni et al., 2012) quantifying latent heat fluxes from the surface as:

$$\lambda E = \lambda \rho \frac{q_s^*(T_s) - q_a}{r_{BL}} \tag{5}$$

where $q_s^*(T_s)$ is the saturated specific humidity at the surface temperature, $q_a = RH \times q_s^*(T_a)$ (kg kg^{-1}) is the overlying air specific humidity, with RH (-) the air relative humidity and $q_s^*(T_a)$ the saturated specific humidity at the air temperature. $r_{BL} = r_{aE} + r_s$ where $r_{aE} = \delta / D$ (s m^{-1}) is the aerodynamic resistance to diffusive water vapor transfer across the viscous sublayer, with D (m^2 s^{-1}) the water vapor diffusion coefficient in free air, and r_s (s m^{-1}) is the soil resistance accounting for soil viscous losses and the effects of soil pore size and spacing between evaporating (water-filled) pores on the evolution of vapor diffusion path as the surface dries (Haghighi et al., 2013; Schlünder, 1988):

$$r_s = \frac{\Gamma}{4k(\theta_{surf})} + \frac{p}{D} \cdot f(\theta_{surf}) \tag{6}$$

where Γ (-) is a proportionality constant reconciling units for capillary liquid to vapor fluxes (see Haghighi et al., 2013 for more detail), $k(\theta_{surf})$ is the unsaturated soil hydraulic conductivity (m s^{-1}) at the surface SM content θ_{surf} (m^3 m^{-3}) (Haghighi et al., 2013; Mualem, 1976), p (m) is the soil mean pore size (estimated as 1/3 of the mean particle size (Glover & Walker, 2009)), and $f(\theta_{surf})$ is a surface-wetness-dependent coefficient accounting for nonlinear interactions influencing vapor diffusion path as the surface dries and spacing between remaining evaporating pores increases (i.e., the evolution of the vapor concentration field from an initially stratified 1-D domain to individual 3-D vapor shells forming over

isolated active pores) (Schlünder, 1988; Shahraeeni et al., 2012):

$$f\left(\theta_{surf}\right)=\frac{1}{2\left(\theta_{surf}-\theta_{res}\right)}-\frac{1}{\sqrt{\pi\left(\theta_{surf}-\theta_{res}\right)}} \tag{7}$$

with θ_{res} ($m^3\ m^{-3}$) the residual SM content. At residual state condition, the water phase is discontinuous and isolated with thin films of water held tightly to the soil grains (Fairbridge & Finkl, 1979). Thus, θ_{res} specifies the maximum amount of water in a soil that does not contribute to liquid flow and surface soil evaporation, and can be estimated from a soil-water characteristic curve model (Luckner et al., 1989).

To facilitate an analytical solution for the equilibrium surface (soil) temperature T_s, we linearize the outgoing longwave radiation $\sigma\varepsilon_s T_s^4$ and saturated specific humidity $q_s^*\left(T_s\right)$ terms around air temperature through truncated Taylor's series as:

$$\sigma\varepsilon_s T_s^4 \approx \sigma\varepsilon_s T_a^4+\left(4\sigma\varepsilon_s T_a^3\cdot\left(T_s-T_a\right)\right) \tag{8}$$

$$q_s^*\left(T_s\right)\approx q_s^*\left(T_a\right)+\left(\frac{c_p}{\lambda}\frac{\Delta}{\gamma}\cdot\left(T_s-T_a\right)\right) \tag{9}$$

where Δ (Pa K^{-1}) is the saturation vapor pressure gradient with temperature and γ (Pa K^{-1}) is the Psychrometric constant. Substituting (2) to (9) into (1) and solving for the state variable T_s yields:

$$T_s=T_a+\frac{\frac{r_{BL}}{r_\psi}-1}{\frac{\rho c_p}{r_{rad}}+\frac{\rho c_p}{r_{aH}}+\frac{\Delta}{\gamma}\frac{\rho c_p}{r_{BL}}+\frac{\rho c_p}{r_g}} \tag{10}$$

where $r_{rad}=\rho c_p\big/4\sigma\varepsilon_s T_a^3$ (s m^{-1}) is the resistance to (longwave) radiative heat flux and r_ψ (s

m^{-1}) is the so-called climatological resistance combining climate variables of saturation deficit and available energy, as a measure of the dominating overhead climatological condition (Lafleur & Rouse, 1988; Raupach, 2001):

$$r_\psi = \frac{\lambda\rho\cdot\left(1-RH\right)\cdot q_s^*\left(T_a\right)}{\Re-\frac{\rho c_p}{r_g}\cdot\left(T_a-\bar{T}\right)} \tag{11}$$

with $\Re=\left(1-\Lambda\right)\cdot R_s-\sigma\varepsilon_s T_a^4\cdot\left(1-\varepsilon_a\right)$. A basic test of the derived surface temperature parametrization in (10) using controlled laboratory-scale data is given in supporting information (Figure S1).

The analytical expression for the equilibrium surface temperature in (10) allows estimation of surface energy balance components, provided surface and routine meteorological variables are available (see Figures S2 to S4 in the supporting information). This analytical solution, which is expressed in terms of resistances representative of surface and climatic mechanisms regulating surface fluxes, allows us to parametrize partitioning of available energy at the soil surface between sensible and latent heat fluxes and thus determine EF as:

$$EF=\frac{\lambda E}{\lambda E+H}=\frac{1}{1+\beta}=\frac{1}{1+\frac{r_{tH}}{r_{aH}}\cdot\left(\frac{r_{BL}}{r_\psi}-1\right)} \tag{12}$$

where $\beta=H/\lambda E$ is the Bowen ratio, and r_{tH}/r_{aH} and r_{BL}/r_ψ are dimensionless groups composed of ratios of resistances accounting for the relative efficiencies of surface energy balance components and (surface-temperature-independent) climatological processes in regulating surface temperature evolution:

$$\frac{r_{aH}}{r_{tH}} = 1 + \frac{r_{aH}}{r_{rad}} + \frac{r_{aH}}{r_g} + \frac{\Delta}{\gamma}\frac{r_{aH}}{r_\psi} = \frac{g_{aH} + g_{rad} + g_g + \frac{\Delta}{\gamma} g_\psi}{g_{aH}} \quad (13)$$

where $g = 1/r$ (m s^{-1}) is referred to as conductance. Note that the dimensionless efficiency terms in (13) are relative to sensible heat flux, and the ratios $(\Delta/\gamma) r_{aH}/r_\psi$ and r_{BL}/r_ψ denote the effectiveness of the surface-independent climate variables relative to sensible and latent heat fluxes, respectively. For given surface and aerodynamic conditions, climate dominates (i.e., $r_\psi \to 0$) sensible and latent heat fluxes under clear sky (i.e., high incoming radiation) and saturated air (resulting in minimal latent heat flux) conditions. As a result, surface temperature evolution is constrained by climatological processes rather than near-surface interactions controlling surface energy fluxes; see section 3.1 for further discussions.

The EF parametrization in (12) complements the conventional formulations based on the Penman-Monteith equation for latent heat flux (e.g., Nichols and Cuenca, 1993) by explicitly addressing the relative efficiency of climatological and surface processes in restoring the state variable of the surface energy balance (i.e., T_s). In addition to EF estimates, the parametrization in (12) facilitates physically based estimates of the Bowen ratio β (-) and the Priestly-Taylor coefficient α_{PT} (-) (Davies & Allen, 1973) (see Figure S5 in the supporting information), with explicit account of the important role of soil and aerodynamic resistances. This is particularly of importance for the attribution of surface temperature anomalies at the regional scale, which is accounted for by the accurate description of dependencies between the Bowen ratio (or the Priestly-Taylor coefficient) and near-surface boundary layer interactions (Rigden & Li, 2017).

2.2. A Generalized EF Framework

Given the multi-dimensional nature of the EF-SM relationship in (12), resulting from the complex (nonlinear) interactions among micrometeorological variables constraining their contribution to energy partitioning at the surface (Gu et al., 2006), the conventional (two-dimensional) EF-SM plane in fact contains multiple curves conditioned on their respective surface and meteorological conditions (Figures 1 and 2a). There is no single or unique curve (as implied from the original EF conceptual framework (Koster et al., 2009; Seneviratne et al., 2010)) characterizing EF-SM relationships under various surface and meteorological conditions (Ford et al., 2014; Schwingshackl et al., 2017). To account for such dependencies, we focus on the two key parameters characterizing EF-SM relationships: (1) the potential (independent of SM) value that EF takes under energy-limited regime (EF_{pot}), and (2) the critical SM θ^* that determines when EF deviates from EF_{pot} and thus transitions from energy-limited to moisture-limited regime (Figure 2a). The asymptotic value of EF under energy-limited regime (EF_{pot}) is not necessarily unity and its value depends on environmental conditions. Provided theoretical estimates of these parameters as functions of surface and meteorological conditions are available, conventional EF-SM framework can be transformed into a "normalized" form with a unique universal curve properly accounting for the multi-dimensional nature of EF-SM relationships as (Figure 2b):

$$\frac{EF}{EF_{pot}} = \begin{cases} 1 & \theta_{surf} \geq \theta^* \\ \dfrac{\theta_{surf} - \theta_{res}}{\theta^* - \theta_{res}} & \theta_{surf} < \theta^* \end{cases} \tag{14}$$

where θ_{res} ($m^3\ m^{-3}$) is the residual SM, EF_{pot} is obtained from (12) at $\theta_{surf} = \theta_{sat}$ with θ_{sat} ($m^3\ m^{-3}$) the saturated SM content, and θ^* is approximated as the SM content at which EF takes 90-95% of its maximal (potential) value, given the convexity of the EF-SM relationship

prescribed by (5) to (7) and (12):

$$\theta^* = \frac{\pi c + 1 - \sqrt{2\pi c + 1}}{2\pi c^2} + \theta_{res} \tag{15}$$

where

$$c = \left(\frac{1-\xi}{\xi}\right) \cdot \frac{\frac{r_\psi}{r_{BL}^{sat}} \cdot \left(\frac{r_{aH}}{r_{tH}} - 1\right) + 1}{p/\delta} \tag{16}$$

with $\xi = 0.9 - 0.95$ and $r_{BL}^{sat} = \delta / D$. Note that the dimensionless ratios in (16) account for the combined and coupled impacts of soil type and meteorological conditions on θ^* and thus on the dominant evaporation regime. Provided surface and routine meteorological measurements are available, the expression for θ^* in (15) and (16) facilitates quantification of the coupling strength between land surface and the atmosphere in the moisture-limited (transitional) regime (Schwingshackl et al., 2017).

We note that the analytical solution in (15) and (16) assumes negligible subsurface viscous losses (i.e., $\Gamma / 4k \approx 0$) imposed on capillary liquid flow towards the vaporization plane at the soil surface. However, such internal losses become important when the land surface water availability is supplied by a shallow groundwater table, with stronger impacts in fine-textured soils subjected to high atmospheric evaporative demand (Haghighi et al., 2013; Lehmann et al., 2008; Shokri & Salvucci, 2011). Hence, a more complete solution for θ^* is obtained from the implicit solution of $EF(\theta) = \xi EF_{pot}$ for θ with $EF_{pot} = EF(\theta_{sat})$.

3. Results and Discussion

3.1. EF Dynamics Controlled by SM and Meteorological Conditions

In the theoretical expression (12), EF is characterized by two dimensionless groups,

r_{aH}/r_{tH} and r_{BL}/r_{ψ}, jointly accounting for the relative contribution of climatological and near-surface processes to the evolution of land surface temperature and thus partitioning of available energy at the land surface. Figures 3 and 4, respectively, show how the ratios r_{aH}/r_{tH} and r_{BL}/r_{ψ} vary as functions of surface and meteorological variables. The ratio r_{aH}/r_{tH} that indicates the relative strength of aerodynamic processes controlling sensible heat flux versus the sum of aerodynamic, radiative, storage and climatological terms is typically larger than unity under a wide range of practical environmental conditions. It approaches unity as wind speed increases especially when saturation deficit is the dominant overhead climatological forcing (i.e., low relative humidity and cloudy sky conditions), implying the dominant role of aerodynamic processes (compared to the other three mechanisms) in dissipating heat and thus the evolution of land surface temperature. . The results reveal that the ratio r_{aH}/r_{tH} is independent of weather conditions (warm vs. cold climate), attributed to the opposite sensitivities of its individual components to air temperature (see the insets). The insets in Figure 3 exhibit corresponding variations in the individual components of the ratio r_{aH}/r_{tH}, with outgoing longwave radiation the least efficient (i.e.,

In contrast to r_{aH}/r_{tH}, the ratio r_{BL}/r_{ψ} that indicates the relative efficiency of climatological processes versus latent heat flux is strongly influenced by weather conditions and surface water availability as well as by sky and wind speed conditions (Figure 4). Figure 4 demonstrates theoretical variations in the ratio r_{BL}/r_{ψ} under various surface and meteorological conditions, revealing its highly dynamic nature (i.e., $r_{BL}/r_{\psi}>1$ or $r_{BL}/r_{\psi}<1$). Note that $r_{BL}/r_{\psi}=1$ implies equal contribution of the dominant climatological forcing (saturation deficit or available energy) and the latent heat flux to surface energy partitioning such that $EF=1$, referred to as isothermal evaporative fraction independent of aerodynamic processes (Raupach, 2001). Boundary layer processes governing turbulent latent heat fluxes are of higher efficiency than the overhead climatological forcing (i.e., $r_{BL}/r_{\psi}<1$ and thus $EF>1$) under relatively high SM and wind speed conditions, especially when saturation deficit (rather than incoming radiation) is the dominant overhead climatological forcing (see the red line under cloudy sky-warm weather condition in Figure 4). Climate's dominance over turbulent latent heat fluxes enhances (i.e., $r_{BL}/r_{\psi}>1$ and thus $EF<1$) as wind speed and SM decrease especially under clear sky conditions (see the blue line under clear sky-cold weather condition in Figure 4).

Note the sensitivity of the ratio r_{BL}/r_{ψ} to SM (i.e., the strength of their relationship) varying substantially with wind speed such that the inflection point of the $r_{BL}/r_{\psi}-SM$ relationship shifts to larger SM values by increasing wind speed. Such nonlinear response of r_{BL}/r_{ψ} to SM variations is attributed to r_{BL} and associated pore-scale mechanisms governing vapor diffusion from soil pores into the atmosphere (see (5)-(7)) (Haghighi & Kirchner, 2017; Haghighi & Or, 2015b; Shahraeeni et al., 2012). In particular, it results from 3D vapor shells forming over individual active evaporating pores as their spacing gradually increases by

surface drying, compensating for the loss of evaporation area by enhancing per-pore fluxes (the so-called compensatory mechanism) (Haghighi & Kirchner, 2017; Shahraeeni et al., 2012). Strong wind speed and/or airflow turbulence conditions, however, result in the formation of a thin viscous sublayer adjacent to the soil surface that restricts full development of the 3D vapor shells and thus r_{BL} continually increases with decreasing SM.

Figure 5 demonstrates the rich dynamics of land surface EF which is constrained by nonlinear (and/or counteractive) interactions among SM and meteorological variables accounted for by the internally linked dimensionless groups r_{aH}/r_{tH} and r_{BL}/r_{ψ} (with shared meteorological variables). When the saturation deficit is the dominant overhead climatological forcing (rather than available energy) and surface evaporation capacity is not limiting to meet the prescribed atmospheric evaporative demand (i.e.,

corresponding increase in the ratio r_{aH}/r_{tH}. Given the different dependencies of the ratios r_{aH}/r_{tH} and r_{BL}/r_{ψ} on the shared micrometeorological variables (as seen in Figures 3 and 4), their rate of variations (and thus their relative contribution to EF variations) differs under various SM and climatic conditions. The theoretical results in figure 5 reveal qualitatively that EF variations would be dominated by the variations in the ratio r_{aH}/r_{tH}, provided

ratio r_{BL}/r_{ψ} in prescribing both EF_{pot} and θ^* for a given region with prescribed soil properties. The ratio r_{aH}/r_{tH} contributes primarily to the EF magnitude and dominates over r_{BL}/r_{ψ} under relatively low SM conditions where sensible heat flux is of higher efficiency than latent heat flux. Overall, mechanisms controlling climatic conditions and latent heat fluxes are the key ones dominating EF-SM dynamics under a wide range of practical conditions.

While EF and its potential value EF_{pot} are notably influenced by climate conditions (Figures 6 and 7), θ^* indicating EF deviations from EF_{pot} (i.e., $EF = \xi EF_{pot}$ marked by red arrows in Figure 6) is of more complex (and rather counteractive) dependencies constraining its variations. This is of profound implications for understanding and determining surface and climatic mechanisms controlling transitions between dominant evaporation regimes under prescribed surface and meteorological conditions (Bagley et al., 2017; Ford et al., 2014; Gentine et al., 2007; Gentine, Entekhabi, et al., 2011; Schwingshackl et al., 2017) . Given the generalized form of the EF-SM relationship depicted in Figure 2, systems with larger or smaller values of the critical SM (θ^*) are, respectively, of higher tendency towards moisture- or energy-limited regimes, with stronger or weaker coupling between the land surface and the atmosphere. Of particular interest are regions straddling the two regimes (i.e., $\theta_{surf} = \theta^*$) where changes in local micrometeorological conditions influencing θ^* would be of substantial impacts on local land-atmosphere feedback processes (Koster et al., 2009; Schwingshackl et al., 2017). Thus, there is an obvious need to determine *a priori* variations in θ^* under atmospheric variability and its likely impacts on local climatic conditions (e.g., persistence of the existing meteorological anomalies and/or occurrence of climate extremes).

To explore complex dependencies embedded in θ^*, Figure 8 shows theoretical variations

in θ^* as a function of three dimensionless groups, p/δ, r_{aH}/r_{tH} and r_ψ/r_{BL}^{sat} in (15) and (16). Generally, θ^* tends to increase when climate condition is favorable to sensible heat flux compared to latent heat flux such that $r_{aH}/r_{tH} \to 1$ and $r_\psi/r_{BL}^{sat} \to 0$ (e.g., cold and humid environment under clear sky condition). In the absence of subsurface viscous losses under hydrostatic conditions, soil limitation to latent heat flux increases by increasing soil pore size (see (5) and (6)) (Lehmann et al., 2008; Or et al., 2013) and thus θ^* further increases in coarse-textured media (i.e., $p/\delta \to 1$). Note the important role of wind speed in supporting both $r_{aH}/r_{tH} \to 1$ and $p/\delta \to 1$ conditions, implying higher sensitivity of θ^* to wind speed than other environmental factors. This is in agreement with the regional-scale results revealing turbulent heat fluxes (and resulting EF estimates) over bare soil locations primarily dominated by wind speed variability (Bertoldi et al., 2007).

Figure 9 explicitly shows the relative strength of different micrometeorological variables in regulating θ^* for a given region. Wind speed and air temperature are the most influential factors affecting θ^* and thus EF estimates over bare soils surfaces (similar to the findings by Bertoldi et al. (2007)) while climate variables of incoming radiation and relative humidity seem to be of minor contribution to the dominant evaporation regime. Nevertheless, θ^* could be influenced by the climate condition (clear versus cloudy), provided land surface is subjected to a relatively dry air layer of high velocity. Variations in air relative humidity would also be important under cloudy sky conditions. Given the complex (nonlinear) interactions among micrometeorological variables constraining their contribution to energy partitioning at the surface (Gu et al., 2006) and eventually to θ^* (Figure 9), further considerations are required prior "generalizing" individual studies performed under prescribed land and atmospheric conditions (e.g., Gentine et al., 2007; Gentine, Entekhabi, et al., 2011; Ford et al., 2014; Bagley et al., 2017).

3.3. Evaluation with Field Observations

Finally, we evaluate the proposed generalized EF framework (Figure 2) and its potential benefits for determining the dominant evaporation regime using field measurements of SM and sensible and latent heat fluxes, as well as routine meteorological variables (i.e., solar radiation, air temperature and relative humidity, and wind speed). Given the low vegetation cover in semiarid regions that results in the soil surface having a substantial influence on the partitioning of energy fluxes at the land surface (with most precipitation input lost as soil evaporation) (Bertoldi et al., 2007; Cavanaugh et al., 2011; Hu et al., 2009; Morillas et al., 2013; Scott & Biederman, 2017; Yepez et al., 2005), we analyzed data from four semiarid sites (see Figure 10) in the early growth stage (MJJ) with minimal vegetation greening.

Results in Figure 10 show how individual realizations (obtained under instantaneously different atmospheric conditions) in the conventional EF-SM plane could systematically be combined in the context of the generalized EF framework. This helps determine the dominant evaporation regime with explicit account of the complex interactions constraining EF-SM relationships. We note that in an ideal setting, the transformed realizations are expected to be collapsed completely along the unique universal curve in the generalized EF framework (see, e.g., model-based transformed EF-SM relationships in Figure S6 in the supporting information with EF values predicted by the model); however, the developed model is of limited predictive capabilities in reproducing observation-based EF values due to uncertainties regarding the neglected role of plant transpiration and/or measurements' quality reflected in the energy balance closure (see Figures S3 and S4 in the supporting information). Thus, model "estimates" of EF_{pot} and/or θ^* for a prescribed set of micrometeorological conditions may not fully account for the corresponding "observed" EF, and as a result the transformed EF scatters over the universal curve.

The transformed EF-SM relationships (right column in Figure 10) explicitly reveal that the selected semiarid regions in Arizona, USA are characterized by a moisture-limited regime during the study period, as widely recognized in the literature (Cavanaugh et al., 2011; Koster et al., 2009; Kurc & Small, 2004, 2007; Schwingshackl et al., 2017; Yepe z et al., 2005). Note the radiation-driven distinction deduced from EF-SM relationships in the conventional plane (left column in Figure 10) that suggests likely changes in the dominant evaporation regime from moisture- to energy-limited regime as the incoming radiation decreases (Ford et al., 2014). Although this seems to be in agreement with our theoretical results in Figure 9 indicating a reduction in θ^* (i.e., moving towards an energy-limited regime) under cloudy sky conditions, such two-dimensional representation of EF-SM relationship does not ensure if the rest of (coupled) meteorological conditions are s ufficient (i.e., an overlaying air layer of relatively high velocity and low saturation – see Figure 9). Explicitly accounting for these complex interdependencies, the generalized EF framework (the right column in Figure 10) reveals the independence of the dominant evaporation regime from incoming radiation, corroborating theoretical and observational findings of Gentine et al. (2007), Gentine, Entekhabi, et al. (2011) and Bagley et al. (2017).

Moreover, the generalized EF framework reveals that the Santa Rita Grassland site was of higher tendency towards (or was about experiencing) energy-limited regime than Walnut Gulch site during the study period, despite the similar range of variations in SM. The results also reveal that the Freeman Ranch site in Texas, USA was occasionally experiencing energy-limited regime as well, with $\theta_{surf}/\theta^* > 1$ under a given set of meteorological conditions. These indicate the important role of environmental variabilities in regulating local land-atmosphere coupling by influencing θ^* and thus system tendency towards either of the evaporation regimes independent of SM, not explicitly acc ounted for by the conventional EF-SM space. To explore more systematically the dependence on other environmental factors,

theoretical estimates of θ^* for the selected sites as a function of measured meteorological variables are presented in Figure 11. The results show the instantaneous nature of the critical SM resulting from varying meteorological conditions in given regions (with prescribed soil properties). The air temperature and wind speed are clearly the dominant factors (the right two columns of Figure 11) in semiarid regions where soil evaporation and its associated mechanisms are of substantial contribution to total exchange rates at the surface (Haghighi & Kirchner, 2017; Hu et al., 2009; Morillas et al., 2013; Scott & Biederman, 2017). Note the opposing effects of air temperature and wind speed on EF estimates (with stronger sensitivity to wind speed, evident from less scattered θ^*–U_a plots) previously recognized over bare soil locations in semiarid regions (Bertoldi et al., 2007). As discussed in section 3.1, the relatively strong influence of wind speed and/or atmospheric turbulence on θ^* results from its contribution to nonlinear interactions governing vapor diffusion processes from soil pores across viscous sublayer (see Figure 4).

Such relatively wide range of variations in θ^* quantified by readily measurable micrometeorological variables (i.e., R_s, T_a, RH, and U_a) provides basis for determining the frequency of the occurrence of moisture- and energy-limited regimes and thus the local dynamics of the land-atmosphere coupling in a given region. Moreover, (predictable) changes in θ^* is of particular importance for quantifying the sensitivity of EF to SM in the moisture-limited regime (quantified by $\partial EF/\partial\theta$) (Haghighi & Kirchner, 2017; Schwingshackl et al., 2017), with implications for land-surface feedbacks to the lower atmosphere (Schwingshackl et al., 2017).

4. Summary and Conclusions

We introduce a generalized framework for evaporative fraction (EF), with explicit incorporation of varying surface and meteorological conditions not accounted for by the

conventional evaporation regime conceptualization. The theoretical basis underlying the conventional EF framework is generally limited to cases where soil moisture (SM) is readily evaporated given sufficient available energy at the land surface, such that EF is neither restricted nor aided by near-surface boundary layer interactions (including subsurface hydraulic properties and above-surface diffusive mechanisms constraining vapor exchanges across the land-atmosphere interface). This is of practical implications for determining land-atmosphere coupling strength in the context of the dominant evaporation regime (energy- versus moisture-limited) (Koster et al., 2009; Seneviratne et al., 2010) and associated impacts on climate extremes and ecosystems (Lorenz et al., 2010; Reichstein et al., 2013; Whan et al., 2015), given observational studies revealing complex environmental dependencies that substantially influence energy partitioning at the surface (Gu et al., 2006) and resulting EF-SM relationships (Bagley et al., 2017; Ford et al., 2014; Koster et al., 2004, 2006; Schwingshackl et al., 2017; Williams & Torn, 2015; Zscheischler et al., 2015) ..

Recent progress in mechanistic modeling of coupled soil moisture-atmospheric controls on surface heat and vapor fluxes (Aminzadeh et al., 2016; Haghighi, 2015; Haghighi & Or, 2015c) provides impetus for developing equations capturing the multi-dimensional nature of EF-SM relationship. Using a mechanistic pore-scale model for bare soil evaporation constrained by surface energy balance, we parametrized the evolution of land surface temperature and the relative efficiency of surface energy balance components in partitioning available energy between sensible and latent heat fluxes, with explicit account of surface and micrometeorological conditions. This parametric framework facilitates a normalized representation of EF-SM relationship characterized by two normalization factors: (1) an asymptotic value (EF_{pot}) that EF takes under non-limiting SM condition for a given set of micrometeorological boundary conditions, and (2) a critical SM (θ^*) that marks the onset of

EF deviation from EF_{pot} (i.e., system transitions from an energy-limited regime to a moisture-limited one). Thus, the projection of the other dimensions (i.e., environmental conditions other than SM) onto the EF-SM plane does not result in scatter, an instead a universal functional form is obtained distinguishing between moisture-limited and energy-limited evaporation regimes (Figure 2).

This study offers physically based estimates of the asymptotic EF (EF_{pot}) and the critical SM (θ^*) as functions of micrometeorological and soil conditions, and provides a robust framework for determining the dominant evaporation regime over bare soil locations. Our results reveal the dominant contribution of wind speed and air temperature, among other environmental factors, to transitions between moisture- and energy-limited regimes (parametrized by θ^*) in regions where soil evaporation and its associated mechanisms are known to play a critical role. The systematic incorporation of complex dependencies in EF-SM relationships into a framework with predictive capabilities potentially reduces much of the empiricism of present approaches quantifying the coupling strength between land surfaces and the atmosphere in the context of the dominant evaporation regime. This is particularly of importance for local regime changes before and during extreme events mostly indirectly detected due to lacking estimates of surface energy fluxes (e.g., Hirschi et al., 2011; Mueller & Seneviratne, 2012; Quesada et al., 2012). Provided measurements (and/or projections) of SM and routine meteorological variables (i.e., solar radiation, air temperature, relative humidity, and wind speed) are available, we envision θ^* as a useful tool to detect (and/or predict) frequency of the occurrence of moisture- and energy-limited regimes in a given region (i.e., $\theta/\theta^* < 1$ or > 1).

Additional tests and further considerations regarding the important role of plant transpiration and associated physiological adjustments in densely vegetated areas, which are

not addressed in this study to retain a simple and practical framework, would be required to assess the general usefulness of the proposed metric at operational scales of hydrologic and climatic interest. Nevertheless, this study provides a physical basis for reconciling independent studies (with seemingly contradictory findings) exploring the effects of incoming radiation and other meteorological conditions on the dominant evaporation regime (e.g., Gentine et al., 2007; Gentine, Entekhabi, et al., 2011; Ford et al., 2014; Bagley et al., 2017); otherwise remains inaccessible with empirical representation of EF-SM relationships.

Acknowledgements

E.H. acknowledges funding from Swiss National Science Foundation (SNSF grant No. P2EZP2-165244). The model data underlying this study can be obtained upon request from the corresponding author at erfanh@mit.edu. Field data used in this study are freely obtainable from http://ameriflux.lbl.gov.

References

Aminzadeh, M., & Or, D. (2014). Energy partitioning dynamics of drying terrestrial surfaces. *Journal of Hydrology*, *519*, 1257–1270. https://doi.org/10.1016/j.jhydrol.2014.08.037

Aminzadeh, M., Roderick, M. L., & Or, D. (2016). A generalized complementary relationship between actual and potential evaporation defined by a reference surface temperature. *Water Resources Research*, *52*(1), 385–406. https://doi.org/10.1002/2015WR017969

Bagley, J. E., Kueppers, L. M., Billesbach, D. P., Williams, I. N., Biraud, S. C. , & Torn, M. S. (2017). The influence of land cover on surface energy partitioning and evaporative fraction regimes in the U.S. Southern Great Plains. *Journal of Geophysical Research: Atmospheres*, *122*(11), 5793–5807. https://doi.org/10.1002/2017JD026740

Bateni, S. M., & Entekhabi, D. (2012). Relative efficiency of land surface energy balance components. *Water Resources Research*, *48*(4), W04510. https://doi.org/10.1029/2011WR011357

Bertoldi, G., Albertson, J. D., Kustas, W. P., Li, F., & Anderson, M. C. (2007). On the opposing roles of air temperature and wind speed variability in flux estimation from remotely sensed land surface states. *Water Resources Research*, *43*(10), W10433. https://doi.org/10.1029/2007WR005911

Brooks, P. D., Chorover, J., Fan, Y., Godsey, S. E., Maxwell, R. M., McNamara, J. P., & Tague, C. (2015). Hydrological partitioning in the critical zone: Recent advances and opportunities for developing transferable understanding of water cycle dynamics. *Water Resources Research*, *51*(9), 6973–6987. https://doi.org/10.1002/2015WR017039

Brutsaert, W. (1975). On a derivable formula for long-wave radiation from clear skies. *Water Resources Research*, *11*(5), 742–744. https://doi.org/10.1029/WR011i005p00742

Budyko, M. I. (1974). *Climate and life*. New York, NY: Academic Press.

Cavanaugh, M. L., Kurc, S. A., & Scott, R. L. (2011). Evapotranspiration partitioning in semiarid shrubland ecosystems: a two-site evaluation of soil moisture control on transpiration. *Ecohydrology*, *4*(5), 671–681. https://doi.org/10.1002/eco.157

Crawford, T. M., & Duchon, C. E. (1999). An improved parameterization for estimating effective atmospheric emissivity for use in calculating daytime downwelling longwave radiation. *Journal of Applied Meteorology*, *38*(4), 474–480. https://doi.org/10.1175/1520-0450(1999)038<0474:AIPFEE>2.0.CO;2

Crow, W. T., Chen, F., Reichle, R. H., & Liu, Q. (2017). L band microwave remote sensing and land data assimilation improve the representation of prestorm soil moisture conditions for hydrologic forecasting. *Geophysical Research Letters*, *44*(11), 5495–5503. https://doi.org/10.1002/2017GL073642

Danckwerts, P. V. (1951). Significance of liquid-film coefficients in gas absorption. *Industrial & Engineering Chemistry*, *43*(6), 1460–1467. https://doi.org/10.1021/ie50498a055

Davies, J. A., & Allen, C. D. (1973). Equilibrium, potential and actual evaporation from cropped surfaces in southern ontario. *Journal of Applied Meteorology*, *12*(4), 649–657. https://doi.org/10.1175/1520-0450(1973)012<0649:EPAAEF>2.0.CO;2

Dirmeyer, P. A., Zeng, F. J., Ducharne, A., Morrill, J. C., & Koster, R. D. (2000). The sensitivity of surface fluxes to soil water content in three land surface schemes. *Journal of Hydrometeorology*, *1*(2), 121–134. https://doi.org/10.1175/1525-7541(2000)001<0121:TSOSFT>2.0.CO;2

Eagleson, P. S. (1978). Climate, soil, and vegetation: 4. The expected value of annual evapotranspiration. *Water Resources Research*, *14*(5), 731–739. https://doi.org/10.1029/WR014i005p00731

Entekhabi, D., Rodriguez-Iturbe, I., & Castelli, F. (1996). Mutual interaction of soil moisture state and atmospheric processes. *Journal of Hydrology*, *184*(1–2), 3–17. https://doi.org/10.1016/0022-1694(95)02965-6

Fairbridge, R. W., & Finkl, C. W. (1979). *The Encyclopedia of soil science*. Dowden, Hutchinson & Ross.

Fischer, E. M., Seneviratne, S. I., Vidale, P. L., Lüthi, D., & Schär, C. (2007). Soil moisture – atmosphere interactions during the 2003 European summer heat wave. *Journal of Climate*, *20*(20), 5081–5099. https://doi.org/10.1175/JCLI4288.1

Ford, T. W., Wulff, C. O., & Quiring, S. M. (2014). Assessment of observed and model - derived soil moisture-evaporative fraction relationships over the United States Southern Great Plains. *Journal of Geophysical Research: Atmospheres*, *119*(11), 6279–6291. https://doi.org/10.1002/2014JD021490

Gao, Z., Russell, E. S., Missik, J. E. C., Huang, M., Chen, X., Strickland, C. E., … Liu, H. (2017). A novel approach to evaluate soil heat flux calculation: An analytical review of nine methods. *Journal of Geophysical Research: Atmospheres*, *122*(13), 6934–6949. https://doi.org/10.1002/2017JD027160

Gentine, P., Entekhabi, D., Chehbouni, A., Boulet, G., & Duchemin, B. (2007). Analysis of evaporative fraction diurnal behaviour. *Agricultural and Forest Meteorology*, *143*(1), 13–29. https://doi.org/10.1016/j.agrformet.2006.11.002

Gentine, P., Polcher, J., & Entekhabi, D. (2011). Harmonic propagation of variability in surface energy balance within a coupled soil-vegetation-atmosphere system. *Water Resources Research*, *47*(5), W05525. https://doi.org/10.1029/2010WR009268

Gentine, P., Entekhabi, D., & Polcher, J. (2011). The diurnal behavior of evaporative fraction in the soil–vegetation–atmospheric boundary layer continuum. *Journal of Hydrometeorology*, *12*(6), 1530–1546. https://doi.org/10.1175/2011JHM1261.1

Glover, P. W., & Walker, E. (2009). Grain-size to effective pore-size transformation derived from electrokinetic theory. *GEOPHYSICS*, *74*(1), E17–E29. https://doi.org/10.1190/1.3033217

Gu, L., Meyers, T., Pallardy, S. G., Hanson, P. J., Yang, B., Heuer, M., … Wullschleger, S. D. (2006). Direct and indirect effects of atmospheric conditions and soil moisture on

surface energy partitioning revealed by a prolonged drought at a temperate forest site. *Journal of Geophysical Research*, *111*(D16), D16102. https://doi.org/10.1029/2006JD007161

Guillod, B. P., Orlowsky, B., Miralles, D. G., Teuling, A. J., & Seneviratne, S. I. (2015). Reconciling spatial and temporal soil moisture effects on afternoon rainfall. *Nature Communications*, *6*, 6443. https://doi.org/10.1038/ncomms7443

Haghighi, E. (2015). *Evaporation from porous surfaces into turbulent airflows: From pores to eddies, Doctoral and Habilitation Theses, 265 pp.* ETH Zurich, Zurich. https://doi.org/10.3929/ethz-a-010489645

Haghighi, E., & Kirchner, J. W. (2017). Near-surface turbulence as a missing link in modeling evapotranspiration-soil moisture relationships. *Water Resources Research*, *53*, 5320–5344. https://doi.org/10.1002/2016WR020111

Haghighi, E., & Or, D. (2013). Evaporation from porous surfaces into turbulent airflows: Coupling eddy characteristics with pore scale vapor diffusion. *Water Resources Research*, *49*, 8432–8442. https://doi.org/10.1002/2012WR013324

Haghighi, E., & Or, D. (2015a). Interactions of bluff-body obstacles with turbulent airflows affecting evaporative fluxes from porous surfaces. *Journal of Hydrology*, *530*, 103–116. https://doi.org/10.1016/j.jhydrol.2015.09.048

Haghighi, E., & Or, D. (2015b). Linking evaporative fluxes from bare soil across surface viscous sublayer with the Monin-Obukhov atmospheric flux-profile estimates. *Journal of Hydrology*, *525*, 684–693. https://doi.org/10.1016/j.jhydrol.2015.04.019

Haghighi, E., & Or, D. (2015c). Thermal signatures of turbulent airflows interacting with evaporating thin porous surfaces. *International Journal of Heat and Mass Transfer*, *87*, 429–446. https://doi.org/10.1016/j.ijheatmasstransfer.2015.04.026

Haghighi, E., Shahraeeni, E., Lehmann, P., & Or, D. (2013). Evaporation rates across a convective air boundary layer are dominated by diffusion. *Water Resources Research*, *49*(3), 1602–1610. https://doi.org/10.1002/wrcr.20166

Hauser, M., Orth, R., & Seneviratne, S. I. (2016). Role of soil moisture versus recent climate change for the 2010 heat wave in western Russia. *Geophysical Research Letters*, *43*(6), 2819–2826. https://doi.org/10.1002/2016GL068036

Higbie, R. (1935). The rate of absorption of a pure gas into a still liquid during short periods of exposure. *Trans. AIChE*, *31*, 365–388.

Hirschi, M., Mueller, B., Dorigo, W., & Seneviratne, S. I. (2014). Using remotely sensed soil moisture for land–atmosphere coupling diagnostics: The role of surface vs. root-zone soil moisture variability. *Remote Sensing of Environment*, *154*, 246–252. https://doi.org/10.1016/j.rse.2014.08.030

Hirschi, M., Seneviratne, S. I., Alexandrov, V., Boberg, F., Boroneant, C., Christensen, O. B., … Stepanek, P. (2011). Observational evidence for soil-moisture impact on hot extremes in southeastern Europe. *Nature Geosci*, *4*, 17–21. https://doi.org/10.1038/NGEO1032

Hu, Z., Yu, G., Zhou, Y., Sun, X., Li, Y., Shi, P., … Li, S. (2009). Partitioning of evapotranspiration and its controls in four grassland ecosystems: Application of a two-source model. *Agricultural and Forest Meteorology*, *149*(9), 1410–1420. https://doi.org/https://doi.org/10.1016/j.agrformet.2009.03.014

Katul, G., Hsieh, C.-I., Oren, R., Ellsworth, D., & Phillips, N. (1996). Latent and sensible heat flux predictions from a uniform pine forest using surface renewal and flux variance methods. *Boundary-Layer Meteorology*, *80*(3), 249–282. Retrieved from https://link.springer.com/content/pdf/10.1007/BF00119545.pdf

Koster, R. D., Schubert, S. D., & Suarez, M. J. (2009). Analyzing the concurrence of meteorological droughts and warm periods, with implications for the determination of evaporative regime. *Journal of Climate*, *22*(12), 3331–3341. https://doi.org/10.1175/2008JCLI2718.1

Koster, R. D., Sud, Y. C., Guo, Z., Dirmeyer, P. A., Bonan, G., Oleson, K. W., … Xue, Y. (2006). GLACE: The global land–atmosphere coupling experiment. Part I: Overview. *Journal of Hydrometeorology*, *7*(4), 590–610. https://doi.org/10.1175/JHM510.1

Koster, R. D., Dirmeyer, P. A., Guo, Z., Bonan, G., Chan, E., Cox, P., … Yamada, T. (2004). Regions of strong coupling between soil moisture and precipitation. *Science*, *305*(5687). Retrieved from http://science.sciencemag.org/content/305/5687/1138

Kurc, S. A., & Small, E. E. (2004). Dynamics of evapotranspiration in semiarid grassland and shrubland ecosystems during the summer monsoon season, central New Mexico. *Water Resources Research*, *40*, W09305. https://doi.org/10.1029/2004WR003068

Kurc, S. A., & Small, E. E. (2007). Soil moisture variations and ecosystem-scale fluxes of water and carbon in semiarid grassland and shrubland. *Water Resources Research*, *43*(6), W06416. https://doi.org/10.1029/2006WR005011

Lafleur, P. M., & Rouse, W. R. (1988). The influence of surface cover and climate on energy partitioning and evaporation in a subarctic wetland. *Boundary-Layer Meteorology*, *44*(4), 327–347. https://doi.org/10.1007/BF00123020

Lehmann, P., Assouline, S., & Or, D. (2008). Characteristic lengths affecting evaporative drying of porous media. *Phys. Rev. E*, *77*(5), 56309. https://doi.org/10.1103/PhysRevE.77.056309

Li, Z., Yang, J., Zheng, Z., Yu, Y., Zhang, T., Hou, X., & Wei, Z. (2016). Comparative study of the soil thermal regime in arid and semi-humid areas. *Environmental Earth Sciences*, *76*(1), 28. https://doi.org/10.1007/s12665-016-6354-2

Lorenz, R., Jaeger, E. B., & Seneviratne, S. I. (2010). Persistence of heat waves and its link to soil moisture memory. *Geophysical Research Letters*, *37*(9), n/a-n/a. https://doi.org/10.1029/2010GL042764

Luckner, L., Van Genuchten, M. T., & Nielsen, D. R. (1989). A consistent set of parametric models for the two-phase flow of immiscible fluids in the subsurface. *Water Resources Research*, *25*(10), 2187–2193. https://doi.org/10.1029/WR025i010p02187

Miralles, D. G., Teuling, A. J., Van Heerwaarden, C. C., & Vilà-Guerau De Arellano, J.

(2014). Mega-heatwave temperatures due to combined soil desiccation and atmospheric heat accumulation. *Nature Geosci*, *7*, 345–349. https://doi.org/10.1038/NGEO2141

Monteith, J. L. (1981). Evaporation and surface temperature. *Quarterly Journal of the Royal Meteorological Society*, *107*(451), 1–27. https://doi.org/10.1002/qj.49710745102

Morillas, L., Leuning, R., Villagarcía, L., García, M., Serrano-Ortiz, P., & Domingo, F. (2013). Improving evapotranspiration estimates in Mediterranean drylands: The role of soil evaporation. *Water Resources Research*, *49*(10), 6572–6586. https://doi.org/10.1002/wrcr.20468

Mualem, Y. (1976). A new model for predicting the hydraulic conductivity of unsaturated porous media. *Water Resources Research*, *12*(3), 513–522. https://doi.org/10.1029/WR012i003p00513

Mueller, B., & Seneviratne, S. I. (2012). Hot days induced by precipitation deficits at the global scale. *Proceedings of the National Academy of Sciences of the United States of America*, *109*(31), 12398–403. https://doi.org/10.1073/pnas.1204330109

Nichols, W. E., & Cuenca, R. H. (1993). Evaluation of the evaporative fraction for parameterization of the surface energy balance. *Water Resources Research*, *29*(11), 3681–3690. https://doi.org/10.1029/93WR01958

Or, D., Lehmann, P., Shahraeeni, E., & Shokri, N. (2013). Advances in soil svaporation physics—A review. *Vadose Zone Journal*, *12*(4). https://doi.org/10.2136/vzj2012.0163

Paw U, K. T., Qiu, J., Su, H.-B., Watanabe, T., & Brunet, Y. (1995). Surface renewal analysis: a new method to obtain scalar fluxes. *Agricultural and Forest Meteorology*, *74*(1–2), 119–137. https://doi.org/10.1016/0168-1923(94)02182-J

Penman, H. L. (1948). Natural evaporation from open water, bare soil and grass. *Proceedings of the Royal Society of London A: Mathematical, Physical and Engineering Sciences*, *193*(1032), 120–145. Retrieved from http://rspa.royalsocietypublishing.org/content/193/1032/120.abstract

Qiu, J., Crow, W. T., Nearing, G. S., Qiu, J., Crow, W. T., & Nearing, G. S. (2016). The impact of vertical measurement depth on the information content of soil moisture for latent heat flux estimation. *Journal of Hydrometeorology*, *17*(9), 2419–2430. https://doi.org/10.1175/JHM-D-16-0044.1

Quesada, B., Vautard, R., Yiou, P., Hirschi, M., & Seneviratne, S. I. (2012). Asymmetric European summer heat predictability from wet and dry southern winters and springs. *Nature Climate Change*, *2*, 736–741. https://doi.org/10.1038/NCLIMATE1536

Raupach, M. R. (2001). Combination theory and equilibrium evaporation. *Quarterly Journal of the Royal Meteorological Society*, *127*(574), 1149–1181. https://doi.org/10.1002/qj.49712757402

Reichstein, M., Bahn, M., Ciais, P., Frank, D., Mahecha, M. D., Seneviratne, S. I., … Wattenbach, M. (2013). Climate extremes and the carbon cycle. *Nature*, *500*. https://doi.org/10.1038/nature12350

Rigden, A. J., & Li, D. (2017). Attribution of surface temperature anomalies induced by land use and land cover changes. *Geophysical Research Letters*, *44*(13), 6814–6822. https://doi.org/10.1002/2017GL073811

Santanello, J. A., Peters-Lidard, C. D., Kumar, S. V., Jr., J. A. S., Peters-Lidard, C. D., & Kumar, S. V. (2011). Diagnosing the sensitivity of local land–atmosphere coupling via the soil moisture–boundary layer interaction. *Journal of Hydrometeorology*, *12*(5), 766–786. https://doi.org/10.1175/JHM-D-10-05014.1

Schlünder, E.-U. (1988). On the mechanism of the constant drying rate period and its relevance to diffusion controlled catalytic gas phase reactions. *Chemical Engineering Science*, *43*(10), 2685–2688. https://doi.org/10.1016/0009-2509(88)80012-5

Schwingshackl, C., Hirschi, M., & Seneviratne, S. I. (2017). Quantifying spatio-temporal variations of soil moisture control on surface energy balance and near-surface air temperature. *Journal of Climate*, JCLI-D-16-0727.1. https://doi.org/10.1175/JCLI-D-16-0727.1

Scott, R. L., & Biederman, J. A. (2017). Partitioning evapotranspiration using long-term carbon dioxide and water vapor fluxes. *Geophysical Research Letters*, *44*(13), 6833–6840. https://doi.org/10.1002/2017GL074324

Seneviratne, S. I., Luthi, D., Litschi, M., & Schar, C. (2006). Land-atmosphere coupling and climate change in Europe. *Nature*, *443*(7108), 205–209. Retrieved from http://dx.doi.org/10.1038/nature05095

Seneviratne, S. I., Wilhelm, M., Stanelle, T., van den Hurk, B., Hagemann, S., Berg, A., … Smith, B. (2013). Impact of soil moisture-climate feedbacks on CMIP5 projections: First results from the GLACE-CMIP5 experiment. *Geophysical Research Letters*, *40*(19), 5212–5217. https://doi.org/10.1002/grl.50956

Seneviratne, S. I., Corti, T., Davin, E. L., Hirschi, M., Jaeger, E. B., Lehner, I., … Teuling, A. J. (2010). Investigating soil moisture–climate interactions in a changing climate: A review. *Earth-Science Reviews*, *99*(3–4), 125–161. https://doi.org/10.1016/j.earscirev.2010.02.004

Shahraeeni, E., & Or, D. (2010). Thermo-evaporative fluxes from heterogeneous porous surfaces resolved by infrared thermography. *Water Resources Research*, *46*, W09511. https://doi.org/10.1029/2009WR008455

Shahraeeni, E., & Or, D. (2011). Quantification of subsurface thermal regimes beneath evaporating porous surfaces. *International Journal of Heat and Mass Transfer*, *54*(19–20), 4193–4202. https://doi.org/10.1016/j.ijheatmasstransfer.2011.05.024

Shahraeeni, E., Lehmann, P., & Or, D. (2012). Coupling of evaporative fluxes from drying porous surfaces with air boundary layer: Characteristics of evaporation from discrete pores. *Water Resources Research*, *48*, W09525. https://doi.org/10.1029/2012WR011857

Shokri, N., & Salvucci, G. D. (2011). Evaporation from porous media in the presence of a water table. *Vadose Zone Journal*, *10*, 1309–1318. https://doi.org/10.2136/vzj2011.0027

Tuttle, S., & Salvucci, G. (2016). Empirical evidence of contrasting soil moisture–

precipitation feedbacks across the United States. *Science*, *352*(6287), 825–828. Retrieved from http://science.sciencemag.org/content/352/6287/825.abstract

Whan, K., Zscheischler, J., Orth, R., Shongwe, M., Rahimi, M., Asare, E. O., & Seneviratne, S. I. (2015). Impact of soil moisture on extreme maximum temperatures in Europe. *Weather and Climate Extremes*, *9*, 57–67. https://doi.org/10.1016/j.wace.2015.05.001

Williams, I. N., & Torn, M. S. (2015). Vegetation controls on surface heat flux partitioning, and land-atmosphere coupling. *Geophysical Research Letters*, *42*(21), 9416–9424. https://doi.org/10.1002/2015GL066305

Yepez, E. A., Huxman, T. E., Ignace, D. D., English, N. B., Weltzin, J. F., Castellanos, A. E., & Williams, D. G. (2005). Dynamics of transpiration and evaporation following a moisture pulse in semiarid grassland: A chamber-based isotope method for partitioning flux components. *Agricultural and Forest Meteorology*, *132*(3–4), 359–376. https://doi.org/10.1016/j.agrformet.2005.09.006

Zscheischler, J., Orth, R., & Seneviratne, S. I. (2015). A submonthly database for detecting changes in vegetation-atmosphere coupling. *Geophysical Research Letters*, *42*(22), 9816–9824. https://doi.org/10.1002/2015GL066563

Tables:

Table 1. List of symbols used in this study

Symbol	Unit	Description
c	–	Model coefficient in (15)
c_p	J kg^{-1} K^{-1}	Specific heat
D	m^2 s^{-1}	Water vapor diffusion coefficient in free air
E	kg m^{-2} s^{-1}	Evaporation flux
EF	–	Evaporative fraction
EF_{pot}	–	Potential evaporative fraction
G	W m^{-2}	Soil vertical conductive heat flux
g	m s^{-1}	Conductance
H	W m^{-2}	Sensible heat flux
K	W m^{-1} K^{-1}	Air/Soil thermal conductivity
k	m s^{-1}	Unsaturated soil hydraulic conductivity
p	m	Soil mean pore size
q_a	kg kg^{-1}	Air specific humidity
q_s^*	kg kg^{-1}	Saturated specific humidity
$\Re$	W m^{-2}	Isothermal net radiation
R_n	W m^{-2}	Net radiation
R_s	W m^{-2}	Incoming shortwave radiation
RH	–	Relative humidity of ambient air
r_{aE}	s m^{-1}	Aerodynamic resistance to latent heat flux
r_{aH}	s m^{-1}	Aerodynamic resistance to sensible heat flux
r_g	s m^{-1}	Resistance to ground heat flux
r_{rad}	s m^{-1}	Resistance to (longwave) radiative heat flux
r_s	s m^{-1}	Soil resistance to latent heat flux
r_ψ	s m^{-1}	Climatological resistance
T	K	Temperature
$\overline{T}$	K	Deep ground temperature
U_a	m s^{-1}	Wind speed
u_*	m s^{-1}	Friction velocity
ν	m^2 s^{-1}	Air kinematic viscosity
Z_T	m	Effective soil thermal thickness
α_{PT}	–	Priestly-Taylor coefficient
β	–	Bowen ratio
δ	m	Viscous sublayer thickness
ε_a	–	Air thermal emissivity

ε_s	–	Soil thermal emissivity
γ	Pa K^{-1}	Psychrometric constant
λ	J kg^{-1}	Latent heat of vaporization
θ^*	m^3 m^{-3}	Critical soil moisture content
θ_{res}	m^3 m^{-3}	Residual soil moisture content
θ_{sat}	m^3 m^{-3}	Saturated soil moisture content
θ_{surf}	m^3 m^{-3}	Surface soil moisture content
ρ	kg m^{-3}	Air density
σ	W m^{-2} K^{-4}	Stefan-Boltzmann constant
ξ	–	Model coefficient in (16)
Δ	Pa K^{-1}	Saturation vapor pressure gradient with temperature
Γ	–	Model coefficient in (6), $O(10^{-5})$
Λ	–	Surface reflectivity/Albedo

Figure Captions:

Figure 1: The variability in the EF-SM space is due to the collapsing a multidimensional dependence in two dimensions. Data marked in red and yellow are conditioned on their respective meteorological conditions, implying that EF-SM relationship is in fact a multi-dimensional function. This has implications for the forced-averaging in the conventional EF-SM space that ignores the physical compatibility of data located in separate spaces, thereby hindering the opportunity to capture dynamic nature of EF-SM relationships (such as likely instantaneous transitions between dominant evaporation regimes) in response to environmental variabilities. Midday half-hourly data (10AM to 4PM) were obtained from Santa Rita Grassland site (Arizona, USA) during spring and summer season of 2010-2015.

Figure 2: (a) Individual realizations in the conventional EF-SM space (in two dimensions) belong to different EF-SM relationships conditioned on their respective meteorological conditions. The individual relationships are characterized by two factors namely potential EF (EF_{pot}) that indicates the asymptotic value of EF under well-watered conditions and a critical SM (θ^*) that marks the inflection point. These key factors vary with other environmental factors not explicitly accounted for by the conventional two-dimensional EF-SM space. (b) The proposed generalized EF-SM plane (in normalized form) that provides a universal relationship to more systematically determining the dominant evaporation regime influenced by environmental variabilities. The schematic exhibits how a given system with prescribed SM content could experience both moisture- and energy-limited evaporation regimes under different sets of meteorological conditions.

Figure 3: Typical variations in the ratio r_{aH}/r_{tH}, accounting for the relative strength of aerodynamic processes versus radiative, storage and climatological processes, with climate variables of relative humidity RH and wind speed U_a under different radiation ($R_s = 1000$

and 400 W m^{-2} for clear and cloudy sky, respectively) and weather ($T_a = 313$, 298, and 283 K for warm, mild and cold weather, respectively) conditions. We note that the representative values used here are for demonstration purposes, providing a typical range of variations in forcing factors under practial field conditions. The insets shown in the second row present the individual components of the ratio r_{aH}/r_{tH} obtained for $RH = 0.5$.

Figure 4: Typical variations in the ratio r_{BL}/r_{ψ}, accounting for the relative efficiency of climatological processes versus boundary layer processes influecing latent heat fluxes, with climate variables of relative humidity RH and wind speed U_a as well as SM (θ_{surf}) under different radiation ($R_s = 1000$ and 400 W m^{-2} for clear and cloudy sky, respectively) and weather ($T_a = 313$, 298, and 283 K for warm, mild and cold weather, respectively) conditions. Dotteld line indicates the isothermal condition (i.e., $T_s = T_a$ and $H = 0$) where latent heat flux and available energy equally contribute to land surafce energy partitioning (i.e., $r_{BL} = r_{\psi}$) and thus $EF = 1$.

Figure 5: Nonlinear interactions among climatic and surface variables, reflected in the two dimensionless groups, determine land surface EF and its dynamics. When surface evaporation capacity and atmospheirc evaporative demand exceed available energy at the surface (i.e., $r_{BL} < r_{\psi}$), the surface receives energy from the convective overlaying air layer (i.e., $H < 0$) to support latent heat exchnage rates at the surface and thus $EF > 1$. Note that EF becomes independent of aerodynamic processes and takes its isothermal value of $EF = 1$ (i.e., $T_s = T_a$ and $H = 0$) when soil hydraulic properties (r_s) meets atmospheirc evaporative demand prescried by aerodynamic (r_{aE}) and climatological (r_{ψ}) processes (i.e., $r_s = r_{\psi} - r_{aE}$).

Figure 6: Typical variations in the two dimensionless groups (i.e., r_{aH}/r_{tH} and r_{BL}/r_{ψ})

governing EF and its dynamics ($EF = 1/(1+\beta)$ with $\beta = r_{tH}/r_{aH}\left(r_{BL}/r_{\psi} - 1\right)$) under clear sky ($R_s = 1000$ W m^{-2}) and various weather conditions ($T_a = 313$, 298, and 283 K for warm, mild and cold weather, respectively). Note the dominant role of the ratio r_{BL}/r_{ψ} (red lines in the left column) in prescribing the inflection point ($EF = \xi EF_{pot}$ marked by red arrows) and magnitude (reflected in lines' order) of EF-SM relationships (right column), especially under relatively high SM content. Under low SM conditons, however, lines' order is reversed and EF magnitude is controlled by the ratio r_{aH}/r_{tH} .

Figure 7: As in Figure 6, but under cloudy sky conditions ($R_s = 400$ W m^{-2}).

Figure 8: Typical variations in the critical SM governed by nonlinear interactions among three dimensionless groups, namely r_{ψ}/r_{BL}^{sat} , r_{aH}/r_{tH} and p/δ. Note that these theoretical results were obtained for a constant residual SM ($\theta_{surf} = 0$) which is known to vary with soil texture (reflected in pore size p) and thus affect critical SM estimates.

Figure 9: Theoretical estimates of the critical SM as a function of climate variables of relative humidity RH and wind speed U_a under different radiation ($R_s = 1000$ and 400 W m^{-2} for clear and cloudy sky, respectively) and weather ($T_a = 313$, 298, and 283 K for warm, mild and cold weather, respectively) conditions. Note the dominant role of wind speed and air tempearture in regulating EF-SM inflection point (θ^*) marking the onset of transition between energy- and soil-moisture limited evaporation regimes.

Figure 10: Original (left) and transformed (right) representation of midday-averaged (10AM to 4PM) EF-SM relationships in four semiarid sites in the early growth stage (MJJ): Santa Rita Grassland (Arizona, USA, 2010-2015), Walnut Gulch (Arizona, USA, 2010-2015), Flagstaff-Wildfire (Arizona, USA, 2007-2010), and Freeman Ranch-Mesquite Juniper

(Texas, USA, 2005-2008). Color shading indicates variations in solar radiation and symbol size refers to wind speed with larger symbols indicating higher wind speed.

Figure 11: Instantaneous variations in the critical SM estimated theoretically using meteorological variable in the selected semiarid regions. Note the dominant (and opposing) control of air temperatu : T_a and wind speed U_a on θ^*.

Figure 1.

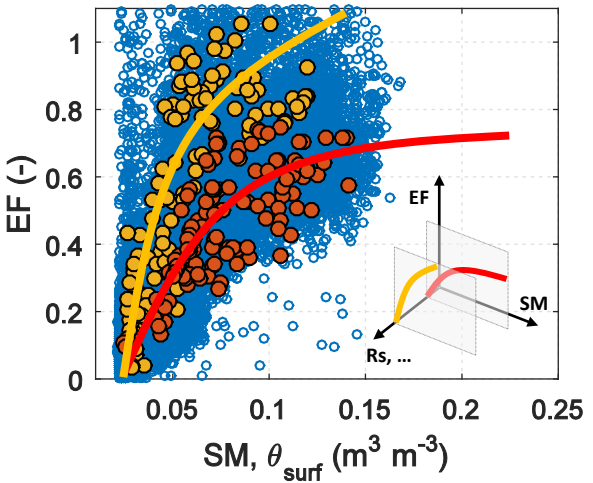

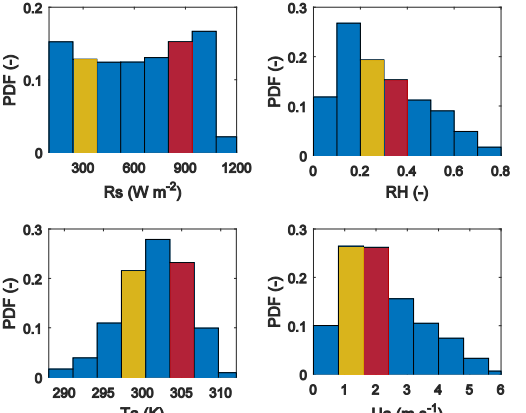

Figure 2.

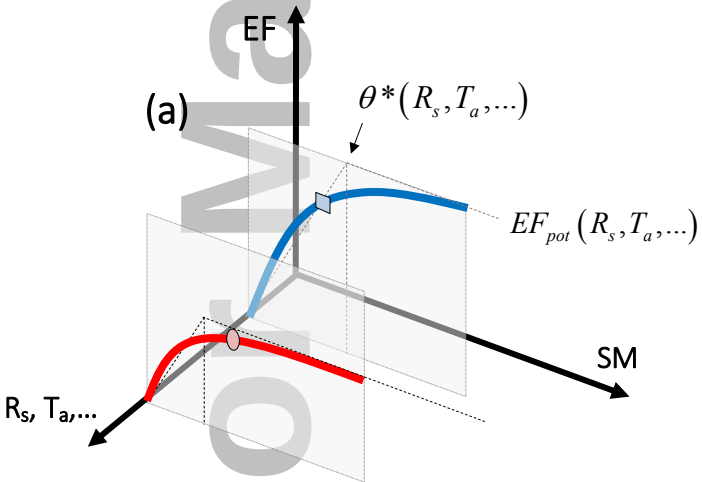

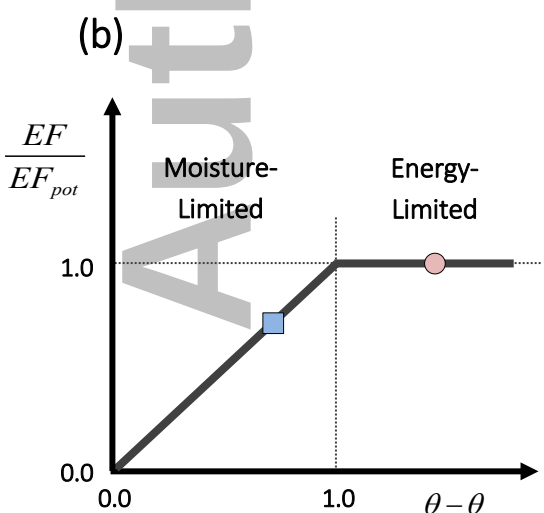

Figure 3.

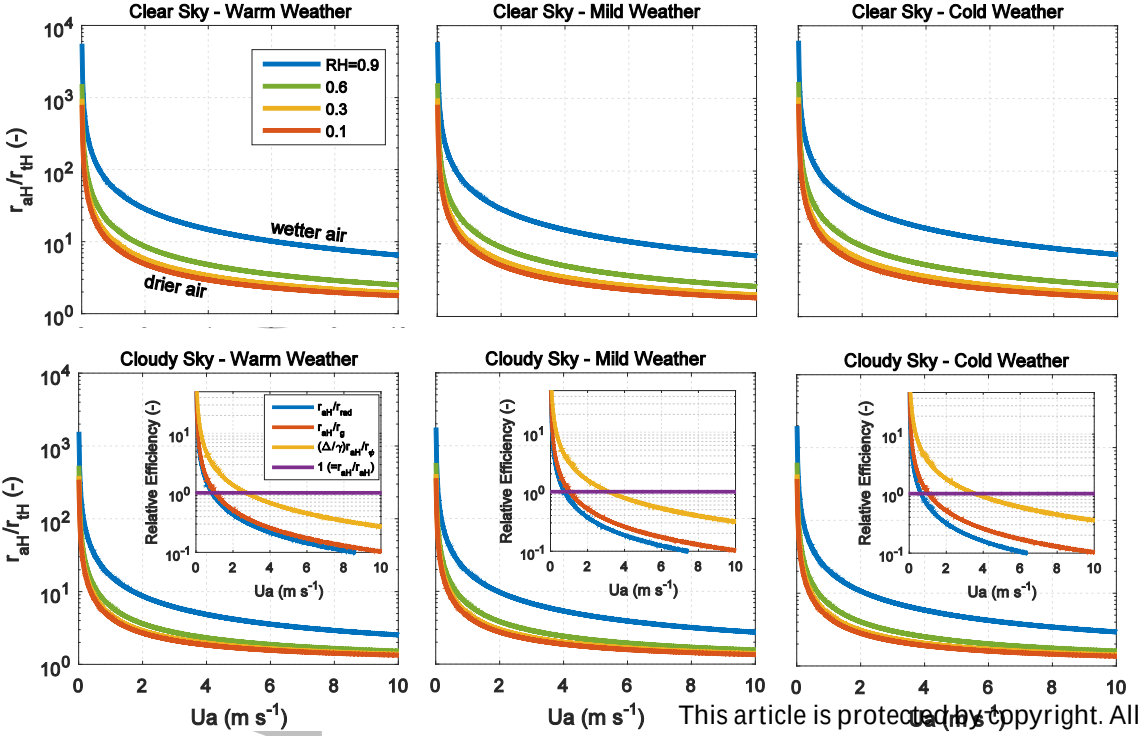

Figure 4.

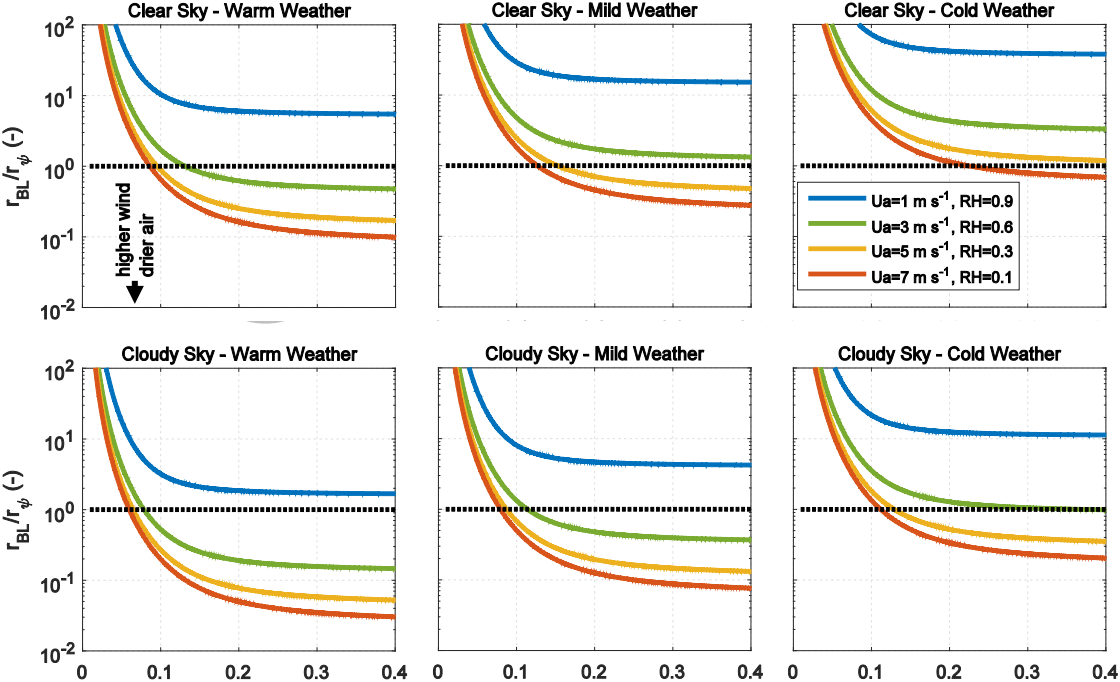

Figure 5.

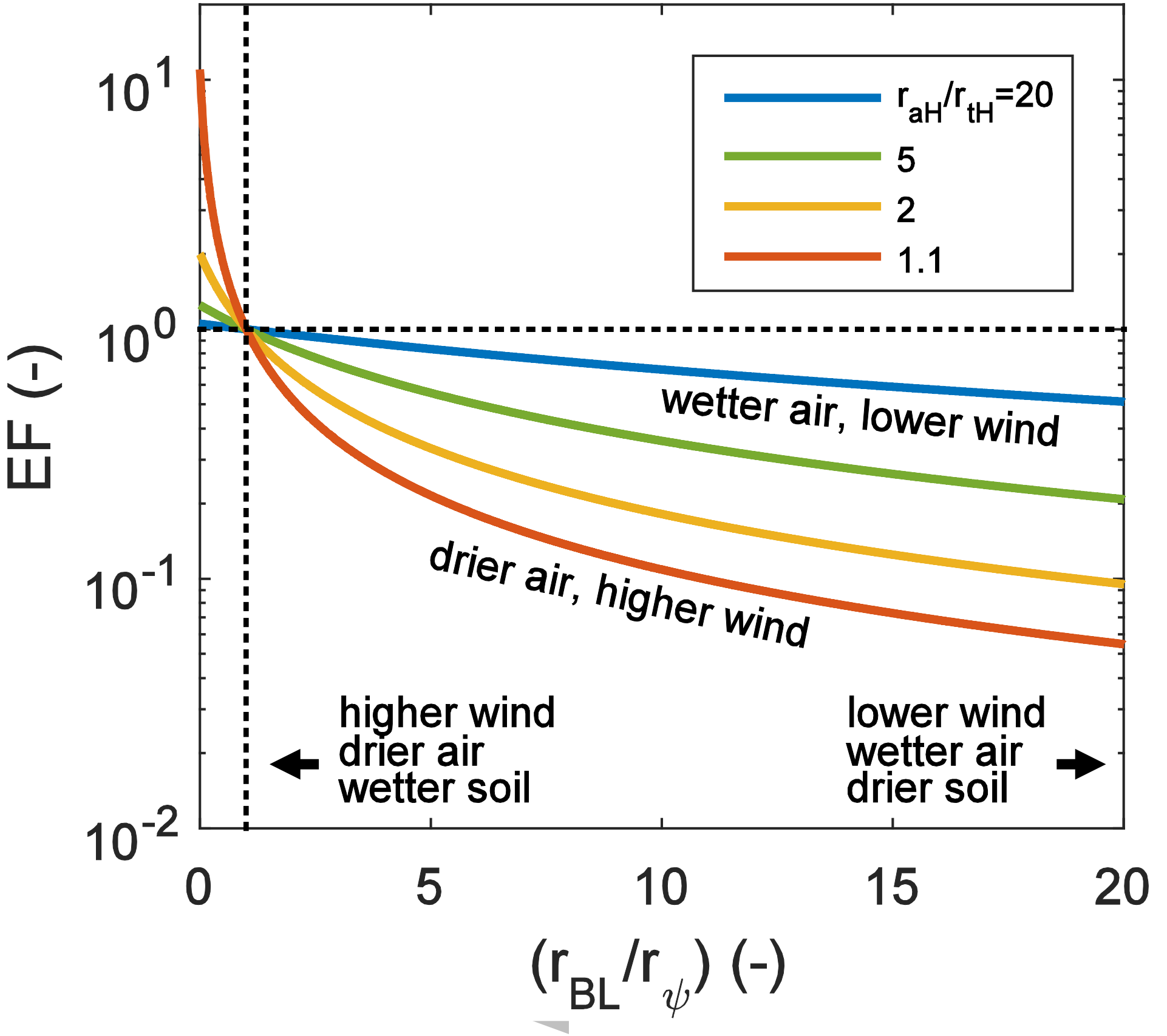
10^1
10^0
10^{-1}
10^{-2}
EF (-)
0
5
10
15
20
(r_{BL}/r_{ψ}) (-)
r_{aH}/r_{tH}=20
5
2
1.1
wetter air, lower wind
drier air, higher wind
higher wind
drier air
wetter soil
lower wind
wetter air
drier soil

Figure 6.

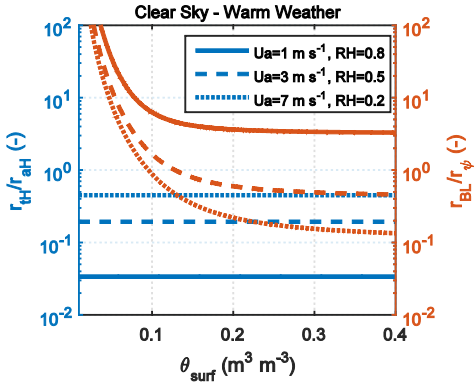

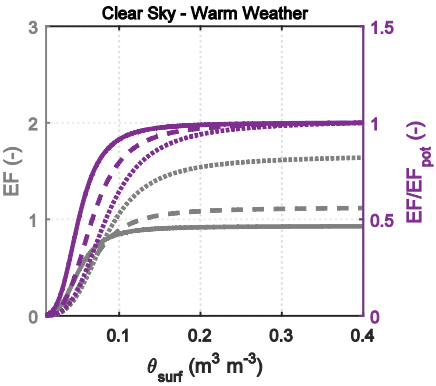

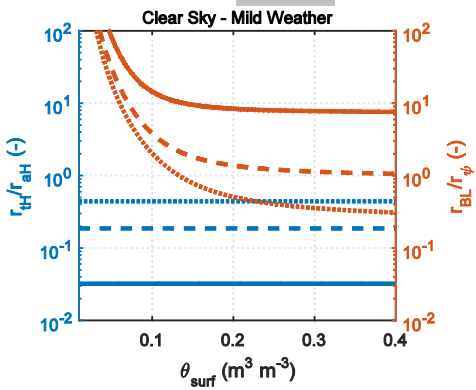

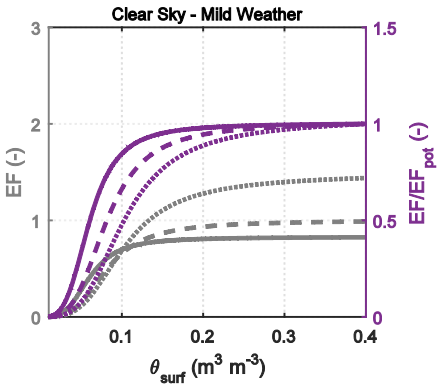

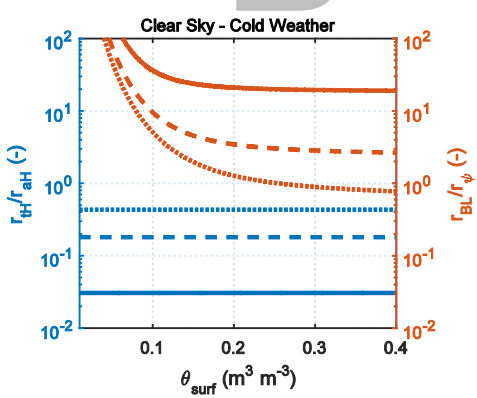

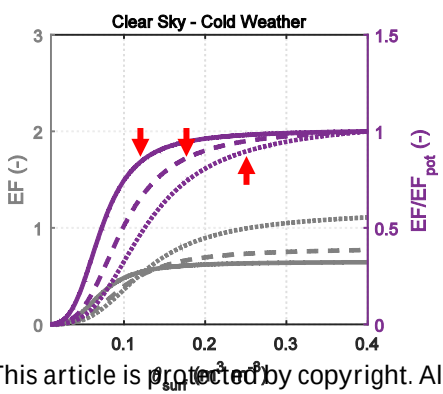

Figure 7.

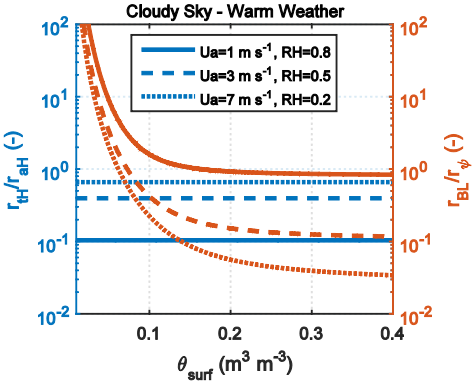

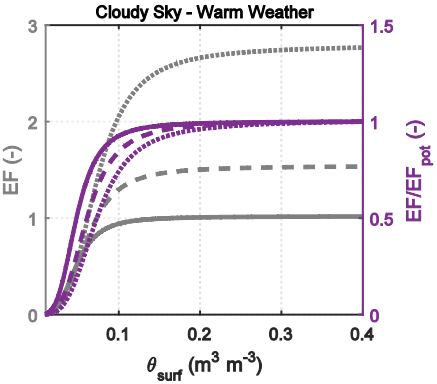

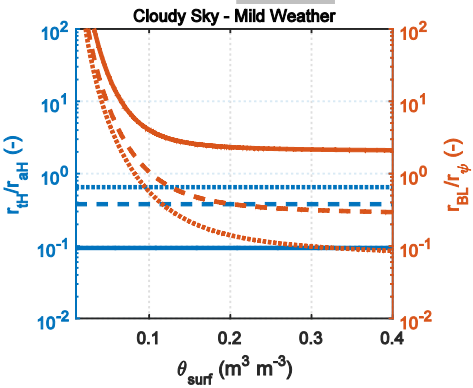

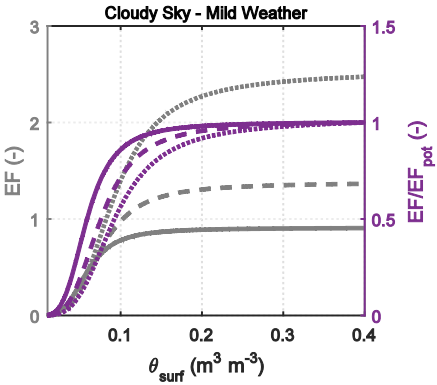

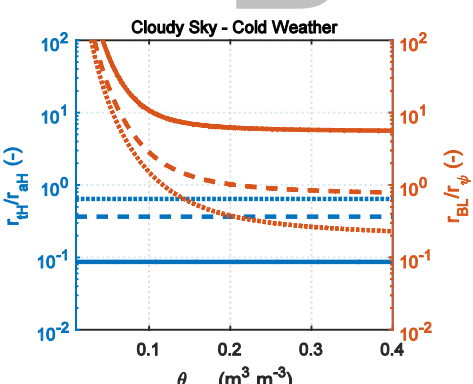

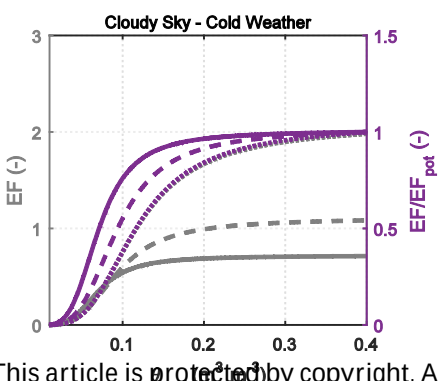

Figure 8.

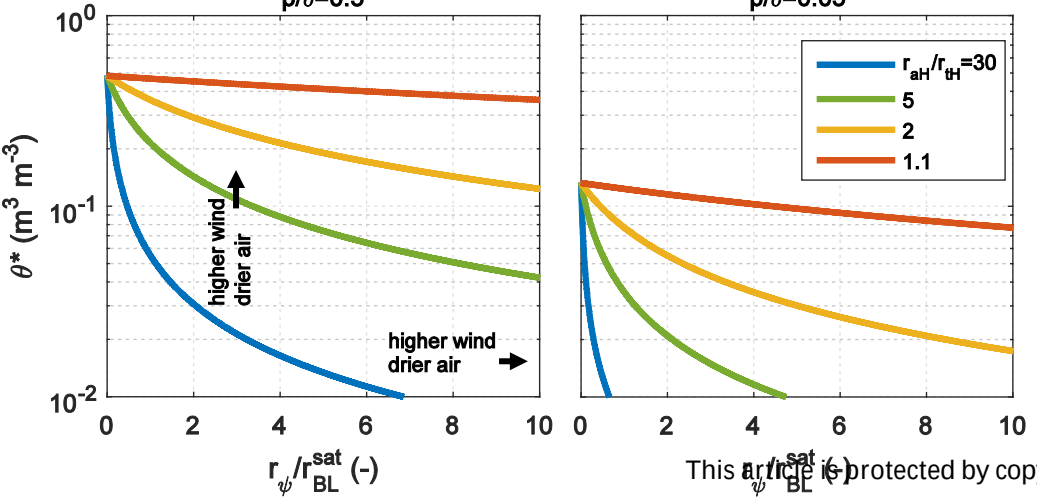

Figure 9.

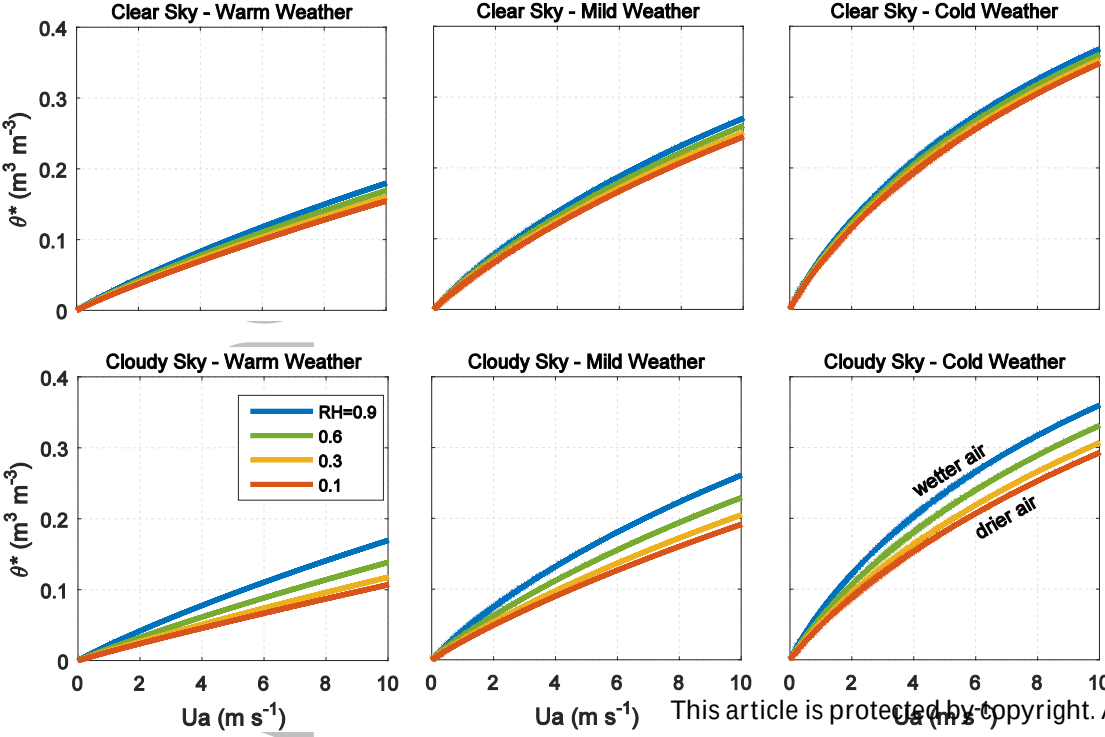

Figure 10.

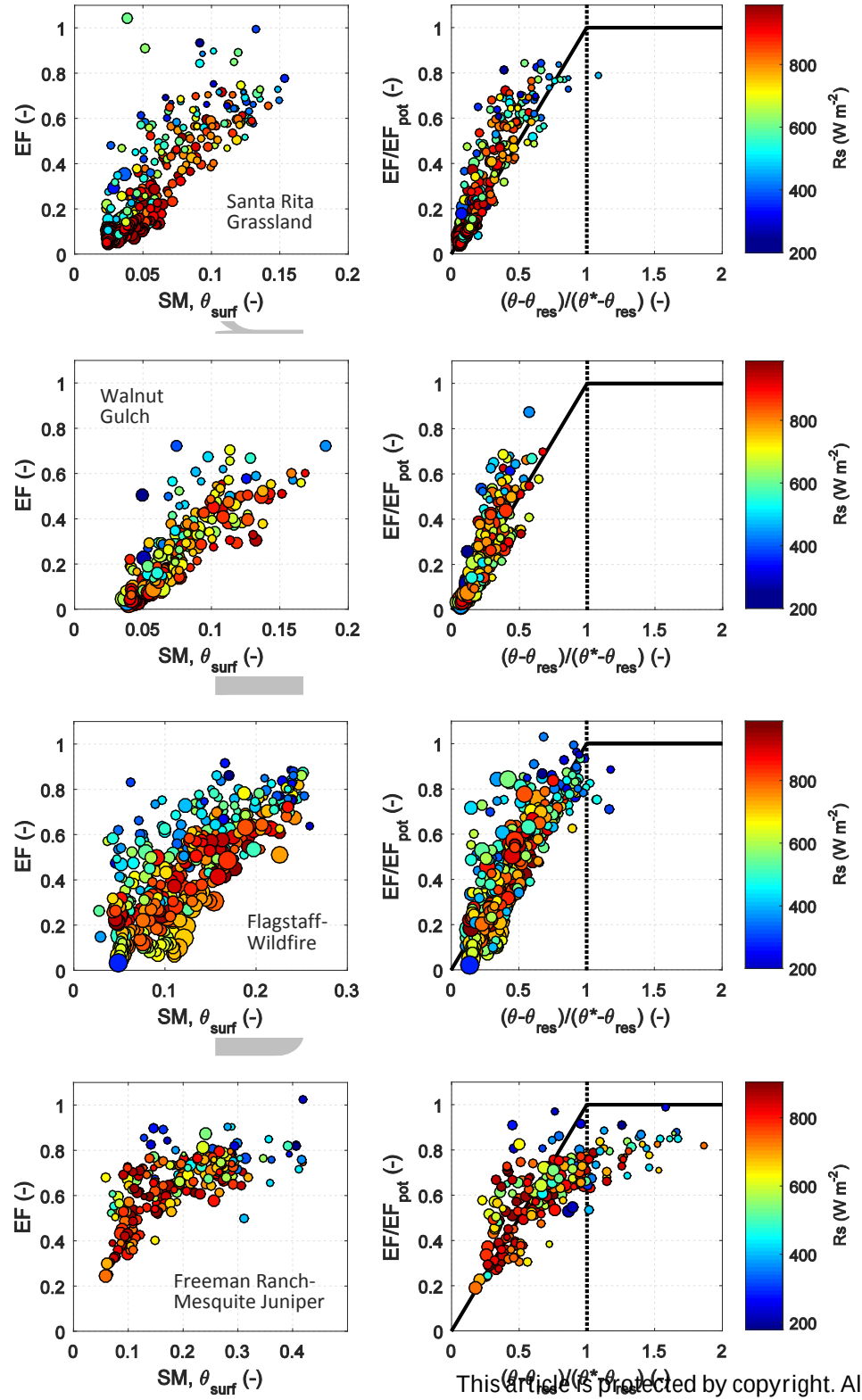

Figure 11.